


Cite this: *RSC Adv.*, 2018, 8, 37804

# Strain-induced conductivity accelerated recoveries in $\text{LaAlO}_3/\text{SrTiO}_3$ heterostructure with millimeter scale†

Xiangqi Wang,<sup>a</sup> Min Zhang,<sup>a</sup> Xirui Tian,<sup>a</sup> Yinying Zhang,<sup>a</sup> Junbo Gong,<sup>a</sup> Azizur Rahman,<sup>a</sup> Rucheng Dai,<sup>\*b</sup> Zhongping Wang<sup>b</sup> and Zengming Zhang <sup>\*bc</sup>

The transport and magnetic properties of  $\text{LaAlO}_3/\text{SrTiO}_3$  (LAO/STO) heterostructure have been studied during cooling and warming. The strain gradient perpendicular to the surface of the heterostructure increases with the thickness of LAO film. The conductivity accelerated recoveries (CAR) are found at 80 K and 176 K in the interface of LAO/STO sample with millimeter scale, and are more obvious for thicker LAO layers during warming. These two recovering temperatures correspond to the migrating energies of oxygen single vacancy and divacancy trapped by polarized domain walls, separately. This indicated that domain walls diffuse along the longitudinal direction and expand to larger area due the strain gradient perpendicular to the interface. The stable and precise accelerating recovering temperatures make the sample at a larger scale a potential widely applied temperature standard reference. The magnetization measurements reveal the coexistence of paramagnetic and diamagnetic in the LAO/STO samples at whole temperature from 2 K to 300 K. The abnormal electric resistance rise is observed with the decreasing temperature below 25 K for the samples of 7 and 15 LAO layers. This anomaly is attributed to the Kondo effect below 25 K and weak anti-localization below 5 K due to the weightier paramagnetic content. The larger diamagnetic content suppresses these contributions in 25 LAO layers sample. This work provided an insightful view that the strain modified structure domain leads to the enhancement of CAR effect, which helps to achieve a better understanding of domain related physics in the LAO/STO system.

Received 16th October 2018  
Accepted 5th November 2018

DOI: 10.1039/c8ra08564a

rsc.li/rsc-advances

## Introduction

The conducting interface between two insulating perovskite materials  $\text{LaAlO}_3$  (LAO) and  $\text{SrTiO}_3$  (STO) has aroused great interest from researchers since Ohtomo and Hwang discovered it in 2004.<sup>1–13</sup> The  $\text{LaAlO}_3/\text{SrTiO}_3$  (LAO/STO) heterointerface has exhibited many unexpected properties such as superconductivity,<sup>2–5</sup> magnetism,<sup>6–8</sup> disorder and localization ground states<sup>9,10</sup> and Rashba spin–orbit interaction *etc.*<sup>11,14</sup> Although the origins of this conducting interface were debated between different groups,<sup>15</sup> the so called ‘polarization catastrophe’ theory is widely recognized by most researchers.<sup>1,16,17</sup> This theory suggests that the discontinuity of the polarization between the polarized layer structure LAO (with sub-layers

$\text{AlO}_2^-/\text{LaO}^+$ ) and non-polarized layer structure STO (with sub-layers  $\text{TiO}_2/\text{SrO}$ ) at the interface could induce the charge transfer from LAO to STO, which should cause the conduction. It successfully explained the phenomenon that a minimum thickness of 4 unit cells (u.c.) LAO layers was required to induce the conduction. In addition to this theory, oxygen vacancies, interfacial strain and atomic mixing were also proposed to possibly induce the interface conductance.<sup>18–23</sup> Furthermore, an enhancement of charge carrier density was found by doping  $\text{LaTiO}_3$  layers into the interface.<sup>24,25</sup> The transport properties can be also modified by doping LAO with magnetic elements.<sup>26</sup>

Magnetotransport studies have revealed that the magnetism of LAO/STO originated from the interface between non-magnetic LAO and STO.<sup>8</sup> The origination of magnetism is unknown yet. Quantum properties such as weak localization, Kondo effect and weak anti-localization have been studied under low temperature,<sup>8–11</sup> and the intrinsic mechanisms are always associated with the electron–electron scattering, electron-local magnetic moment scattering, spin-orbital scattering *etc.* Disorder and localization play the important roles in these quantum effects at low temperature.

The previous investigations mainly focused on the ground state of the heterostructure to seek for the quantum properties

<sup>a</sup>Department of Physics, University of Science and Technology of China, Hefei 230026, China

<sup>b</sup>The Centre for Physical Experiments, University of Science and Technology of China, Hefei 230026, China. E-mail: zzm@ustc.edu.cn; dairc@ustc.edu.cn

<sup>c</sup>Key Laboratory of Strongly-Coupled Quantum Matter Physics, Chinese Academy of Sciences, School of Physical Sciences, University of Science and Technology of China, Hefei, Anhui 230026, China

† Electronic supplementary information (ESI) available. See DOI: 10.1039/c8ra08564a



near the temperature of absolute zero. Under such a purpose researchers only concerned with the heterointerface during cooling, not the inverse warming process. STO exists structure transition from cubic to tetragonal phase at around 105 K during cooling.<sup>27</sup> The structure transition of STO leads the abundant structure domain on STO surface.<sup>28–31</sup> Kalisky and Moler *et al.*<sup>29</sup> used superconducting quantum interference device (SQUID) to measure the localized magnetic field, and found the domain structure strongly modified the local conductivity, which showed as the current intensity increases along the domain walls. Roy and Klein *et al.* also found the current-induced nonuniform enhancement of sheet resistance due to the interaction between domain walls and oxygen vacancies in STO.<sup>28</sup> Erlich *et al.*<sup>30</sup> confirmed the channel behavior of conductivity by using the polarized light microscopy technology. Ma *et al.*<sup>31</sup> carried out SEM imaging at low temperature and found that the ferroelectric can be induced within the twin walls in STO beyond the critical electrical field. However the above works yield no results on transport properties. To understand the role of domain structure, it needs to consider the transport properties influenced by the domain structure and how the LAO layers affect the domain structure.

In this work, we focused on the electrical transport and magnetic properties during warming process after cooling to 2 K. Temperature dependent transport, magnetoresistance and magnetization properties were measured for different thicknesses of LAO films grown on STO for both cooling and warming.

## Experiment details

The  $\text{LaAlO}_3$  thin films in this work were grown on  $\text{TiO}_2$  terminated (100)  $\text{SrTiO}_3$  substrate in  $10^{-4}$  mbar pressure of  $\text{O}_2$  and at

1073 K using pulsed laser deposition technique. To control the thickness with sub-u.c. precision, film growth was monitored *in situ* using reflection high energy electron diffraction (RHEED). The samples were kept in the  $\text{O}_2$  atmosphere when cooling to room temperature. The Scanning Electron Microscope (SEM, Hitachi S-4800) with energy dispersive spectroscopy (EDS) was used for elemental mapping. The results of La, Al and O elemental mapping images are shown in Fig. S1,<sup>†</sup> which indicates the successful formation of LAO film. The X-ray photoelectron spectroscopy (XPS) was measured using ESCALAB 250 from Thermo-VG Scientific. The XPS results are displayed in Fig. S2.<sup>†</sup> The Al 2p, O 1s and La 3d peaks can be seen in the figure. No shift of the peaks is observed, which reveal no change of chemical state.

X-ray diffraction and reciprocal space mapping (RSM) with  $\text{Cu-K}\alpha$  radiation (Rigaku, TTR III) was used for characterization of film growth. The STO (311) and LAO (311) planes were chosen for RSM measurement. Transport properties were tested using physical property measurement system (PPMS) from Quantum Design Company with a typical four wire electrode in the length scale of several mm which plunges into the interface. The resistance is measured through a cycle of cooling and warming between 300 K and 2 K. Magnetic properties were tested using magnetic property measurement system (MPMS) through cooling and warming between 300 K and 2 K with a field of 0.01 T.

## Results and discussion

Fig. 1(a) is the schematic diagram for the heterostructure of  $\text{LaAlO}_3$  on  $(\text{TiO}_2)^0$  terminated  $\text{SrTiO}_3$ . The perovskite oxides  $\text{LaAlO}_3$  and  $\text{SrTiO}_3$  show similar layer structure with lattice constants 3.789 Å and 3.905 Å, respectively. The  $\text{SrTiO}_3$

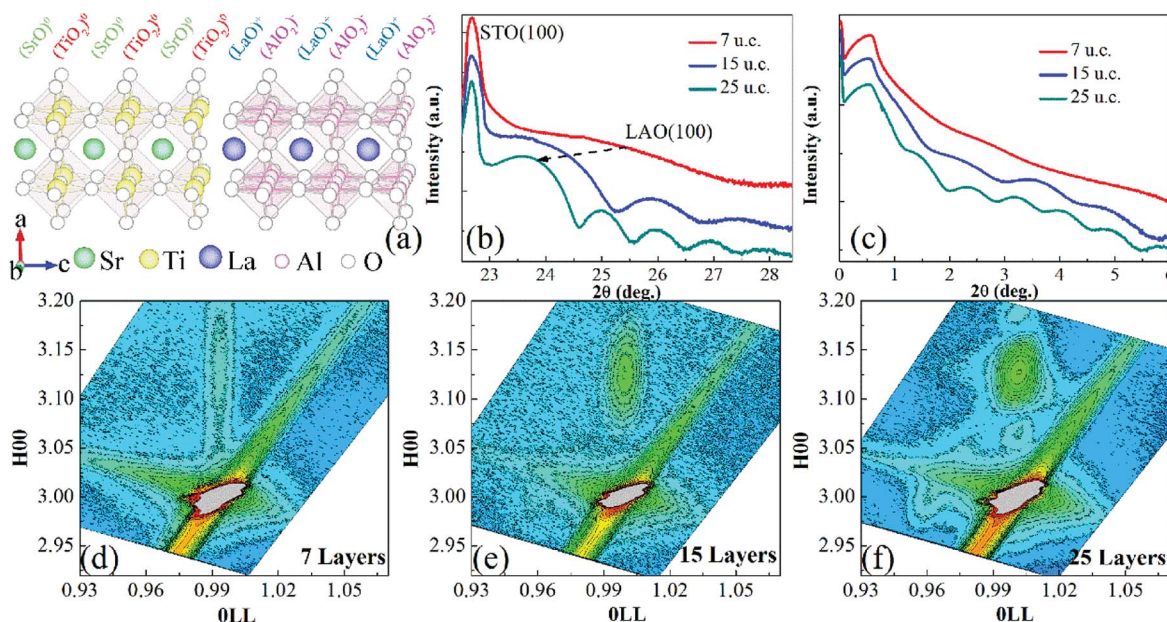


Fig. 1 (a) Structure schematic diagram of  $\text{LaAlO}_3$  on  $(\text{TiO}_2)^0$  terminated  $\text{SrTiO}_3$  heterostructure. (b) X-ray diffraction results for different thicknesses of LAO/STO at angles around (001) peak. (c) X-ray reflection results for different thicknesses LAO/STO samples at 0–6 degree. (d)–(f) Reciprocal space mapping of the (311) plane of LAO/STO. Both structure information of in-plane (H00) and out-of-plane (0LL) are observed.



**Table 1** LaAlO<sub>3</sub> thickness and lattice constants derived from XRR and RSM measurement results

	Theoretical thickness	XRR results	RSM: out-of-plane	RSM: in-plane
7 u.c.	2.66 nm	2.94 nm	3.734 Å	3.905 Å
15 u.c.	5.70 nm	6.61 nm	3.745 Å	3.905 Å
25 u.c.	9.50 nm	10.13 nm	3.746 Å	3.898 Å

consisted of two non-polar sublayers, (SrO)<sup>0</sup> and (TiO<sub>2</sub>)<sup>0</sup>, while LaAlO<sub>3</sub> is formed by two polar sublayers, (LaO)<sup>+</sup> and (AlO<sub>2</sub>)<sup>-</sup>.<sup>4</sup> Fig. 1(b) presents the XRD patterns for LAO/STO films with thickness of 7, 15 and 25 layers (also unit cells), respectively. The patterns around (100) of LAO indicate that LAO layers are epitaxially grown on the STO single crystal substrate along the (100) orientation. The LAO (100) diffraction peak shows a clear shift to lower angle with the increasing thickness, which reveals the lattice strain gradually releases. Fig. 1(c) shows the small angle X-ray reflection (XRR) for all the prepared LAO/STO thin films. It can be seen from XRR results that the period of finite size Fresnel oscillation around the diffraction peak varies with the thickness of LAO film. This permits us to determine the thickness by using the well-known Bragg equation:  $2d \sin \theta = n\lambda$ , where  $d$  and  $\lambda$  stand for thickness of LAO thin film and wavelength of X-ray, respectively. We also calculated the thickness of the as-prepared LAO/STO samples remarked by the number of unit cells (u.c.) “ $n$ ” obtained by RHEED intensity oscillations and the bulk lattice constant of 0.38 nm of LAO, the thickness was estimated to be  $n \times 0.38$  nm. Our calculated values are consistent with the XRR results as presented in Table 1.

The reciprocal space mapping (RSM) technique is employed to study the interfacial strain dynamics with increasing thickness of LAO/STO film. The (311) planes of both LAO and STO were chosen for the observation of both in-plane (0LL) and out-of-plane (H00) information. Fig. 1(d–f) display the RSM images for the prepared LAO/STO epitaxial films. These results allow us to calibrate the LAO lattice constants comparing with standard single-crystal STO substrate, the outcomes are shown in Table 1. As for the 7 u.c. layers of LAO film, the (0LL) in-plane direction shows no obvious difference from the substrate, suggesting the growth is in the plan lattice parameters similar to the substrate and can be considered as fully strained. Furthermore, the LAO (H00) out-of-plane direction shows a broad diffraction profile for this ultrathin film, which confirms the formation of highly strained interface between substrate and epitaxial film. When the number of LAO layers increases, the diffraction profiles of LAO and STO gradually separate each other. This indicates the formation of a gradually relaxed interface. Quantitative calculation results also exhibit such changeover in Table 1. So the RSM results clearly reveal that the LAO/STO interface strain varies from fully strained state to a partial strained state with the increasing layers of LAO film.

Fig. 2 is the transport properties of the interfaces between different LAO layers and STO substrate. The resistance is tested against temperature for both cooling and warming. During warming up, two anomalies in  $R$ – $T$  curves are found for 15 u.c.

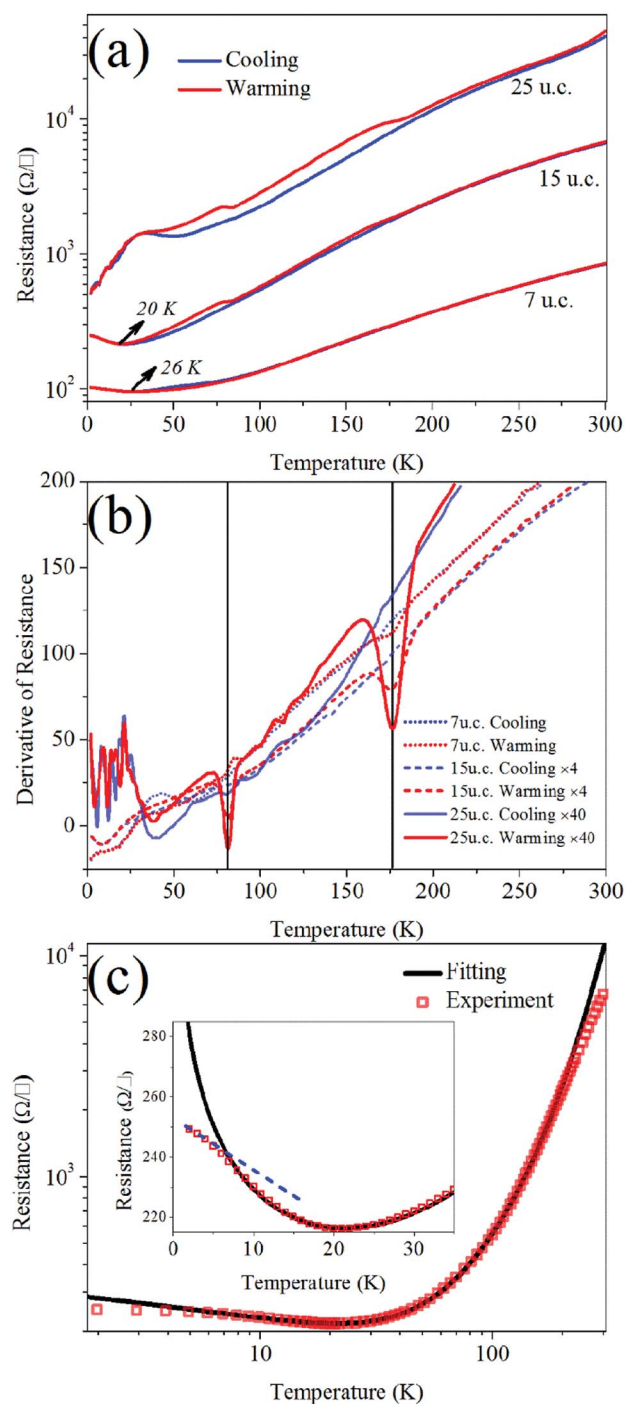


**Fig. 2** (a) Transport properties for LAO/STO samples with different layers LAO. The sheet resistance is measured in the process of cooling and warming. The arrows indicate the Kondo temperatures for 7 u.c. and 15 u.c. samples. (b) Derivative curve of the temperature dependent sheet resistance for LAO/STO samples. (c) Fitting result of 15 u.c. LAO/STO interface sheet resistance during cooling. Inset: saturation of the logarithmic term, which is contribution of spin-orbital scattering.

and 25 u.c. samples. The resistance temporarily deviates the rising trend at 80 K and 176 K. Within a little temperature region about 5 K, the conductivity is enhanced and then declined. The two inflection points indicate that the sample undergoes a conductivity accelerating recovering (CAR) process.





As observed in Fig. 2(a), the two deviations are more obvious for more layers of LAO/STO. The derivative curves of resistance are shown in Fig. 2(b). It can be seen that the two derivative valleys always appear at the same temperatures for different samples, which shows high stability. Similar anomalies have also been observed in the patterned LAO/STO and STO samples with the length scale of several  $\mu\text{m}$ .<sup>28,32,33</sup> The anomalies presenting in these references significantly enhance when the sample length decreases to nm scale, the previous works considered that the anomalies could only occur in several u.c. layers LAO/STO samples with length scale of micron.<sup>34</sup> The small scale limited the wide application from the anomaly property. Contrary to the previous conclusion, in our current work the anomalies can also appear in large length scale of several mm with increasing the number of LAO layers. Because this two novel points are of the precise temperature interval it provides a potential temperature standard reference in the region of low temperature based on its resistance measurement and can be widely applied due to its larger scale.

Minhas *et al.*<sup>34</sup> made nano-patterned 6 u.c. layers LAO/STO samples and observed giant resistance anomaly. The anomaly is explained as the current, which flows along the domain wall, is interrupted near the structure transition region of STO. However the theory comes to a conclusion that the anomalies cannot appear for large scale sample, which suggests more mechanisms need to be introduced. The domain wall can be generated by the structure transition from cubic to tetragonal at 105 K for STO during cooling. It is clear that the carriers such as oxygen vacancies were firstly trapped in the vicinity of the domain wall with the further cooling. The two recoveries correspond to two times of release for the carriers. Seri *et al.*<sup>33</sup> determined the two trapping energy barriers  $E_{b1}$  and  $E_{b2}$  from less than 10  $\mu\text{m}$  patterned 4 u.c. LAO/STO sample. Roy *et al.*<sup>28</sup> also found two accelerated conductivity recoveries in  $\text{Ar}^+$ -irradiated  $\text{SrTiO}_3$ . They considered that the two trapping energy barriers perfectly match the migrating energies of oxygen single vacancies and divacancies. At low temperature, comparing to the current of 40  $\mu\text{A}$  in Seri group's work, the larger current of 8 mA in this work strongly polarized the domain walls, which attract the vacancies around the domain walls. The trapped single-vacancies and divacancies become mobile above 80 K and 176 K, which yields the conductivity recovery, separately. The reported cases<sup>28,32–34</sup> are the patterned few layers LAO/STO in the length scale less than 10  $\mu\text{m}$ , which means the interface is fully strained. When the number of LAO layers increases, the sample changes from fully strained state to partial strained state. The vertical strain gradient of the sample increases and leads to the longitudinal diffusion of the domain and furtherly expands the network of the domain in plane and enlarges the domain formation area. The larger domain area and deep diffusion of the domain makes the accelerated recoveries of conductivity more obviously observed in the current case. It is worth emphasizing that preparation condition also plays the key role in observing the CAR. Ariando *et al.*<sup>7</sup> also made the 10 u.c. LAO/STO sample in length scale of several mm, however they did not observe the CAR in the resistance curves. The electronic phase formation of 2-dimension electron gas in the

interface is greatly affected by the oxygen pressure, the annealing temperature and other detail factors in the preparing process.

In the cryogenic region, the resistance shows the abnormal rising behavior with decreasing temperature as seen in Fig. 2(a). This behavior is attributed to the spin scattering of the conducting electrons interacting with localized magnetic moments at the interface.<sup>6–8</sup> The temperature dependence of resistance is helpful to understand the nature of the scattering. The  $R$ - $T$  curves for 7 u.c. and 15 u.c. samples are in logarithmic relationship and can be described well by:

$$R_s = a \ln\left(\frac{T}{T_{\text{eff}}}\right) + bT^2 + cT^5,$$

where first term of right side stands for the contribution of Kondo effect,  $T^2$  and  $T^5$  terms are response to electron–electron and electron–phonon scatterings, respectively.<sup>8</sup> The fitting for 15 u.c. sample is shown in Fig. 2(c). The logarithmic curve is dominated by Kondo effect from the interaction between conducting carriers and localized magnetic moment. The experimental curve is found to be saturation at around 5 K as seen in inset of Fig. 2(c). We consider that this is the contribution of weak anti-localization induced by spin-orbital scattering, which is discussed in the following part. This is worth mentioning that the Kondo temperature ( $T_{\text{eff}}$ ) is shifting towards lower values as the thickness of the LAO thin film increases, in the current work they are 26 K for 15 u.c. LAO and 20 K for 7 u.c. LAO as pointed out in Fig. 2(a), separately. As for sample with 25 u.c. layers, its resistance shows a reverse trend and decreases with the further cooling below 25 K. Its temperature derivative of resistance reveals the conducting fluctuation below 40 K.

To test the magnetic behavior of the LAO/STO heterostructure, the magnetization measurement was carried out in the temperature range between room temperature and 2 K under the magnetic field of 0.01 T, as shown in Fig. 3. As the LAO and STO are both diamagnetic perovskites, the fascinating feature of this measurement is the low temperature diamagnetic to paramagnetic transition for 7 u.c. and 15 u.c. samples. The magnetization is almost a straight platform and with the negative value at high temperature, shows the diamagnetic property. Below a critical temperature, the magnetization value start to increase and then with a sharp increase, which shows an upturn and becomes positive. The similar trend is also observed for the 25 u.c. sample, but negative magnetization exists for whole temperature. This conclusion is different with Ariando's work.<sup>7</sup> Ariando *et al.* found the ferromagnetic phase exists in LAO/STO for whole temperature range. This distinction reveals the important pole of preparing conditions again. To analysis the measured magnetization curves, we divide the contribution of the magnetization into two terms, the paramagnetic term and diamagnetic term. The results are fitted using the following formula:  $M = \frac{C}{T} + M_d$ , the first term is the contribution of paramagnetic while the second one is response to the diamagnetic term. The fitting results are shown in Fig. 3(a). The fitting curves are in good agreement with the experiment results, which demonstrate that the samples are coexistence of paramagnetic and diamagnetic in whole temperature region. The



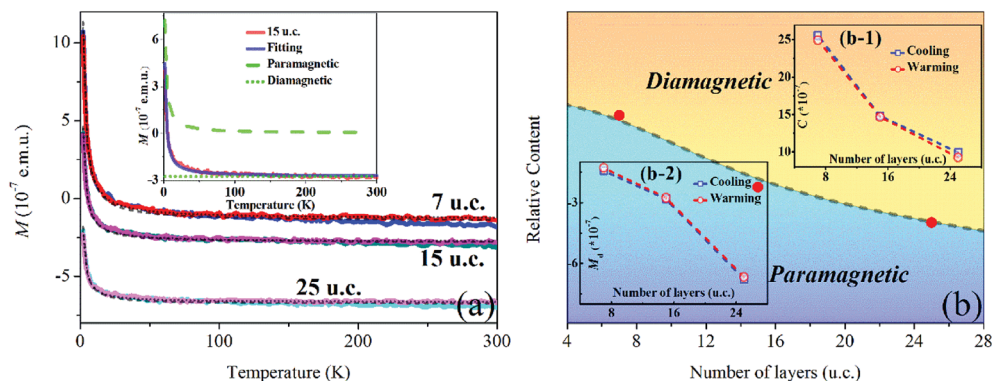


Fig. 3 (a) Magnetization for different LAO/STO samples. The measurement is tested for both cooling (blue, dark cyan and cyan curves for 7, 15 and 25 u.c. samples, respectively) and warming (red, magenta and LT magenta curves for 7, 15 and 25 u.c. samples, respectively) at a field of 0.01 T. Black dash and dot curves show the fitting results for cooling and warming, respectively. (b) Relative content of diamagnetic and paramagnetic for different LAO layers samples. The insets of (b-1) and (b-2) show the fitting parameters for different samples.

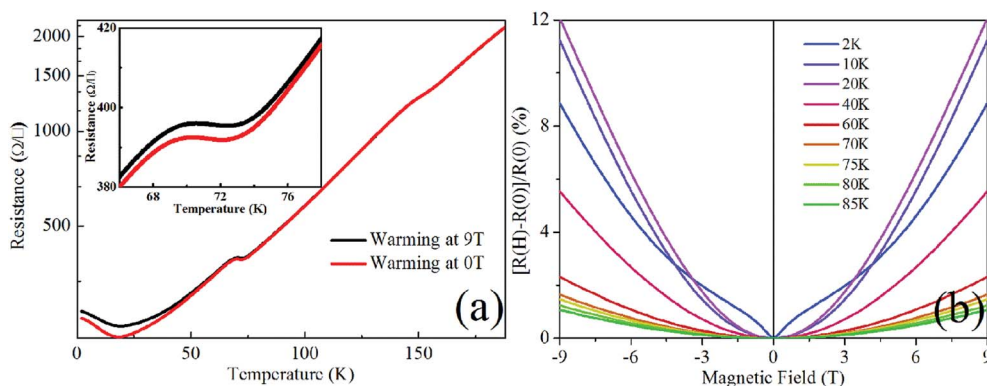


Fig. 4 Magnetoresistance of 15 u.c. LAO/STO interface. (a) Sheet resistance of warming at 0 T and 9 T. (b) Magnetoresistance at different temperature during warming from 9 T to  $-9$  T.

cooling and warming magnetization curves shows no obvious difference. The relative content of paramagnetic and diamagnetic is shown in Fig. 3(b). With the increasing of LAO layers, the paramagnetic ratio increase and the diamagnetic ratio decrease. The corresponding fitting parameters are shown as insets of (b-1) and (b-2) in Fig. 3. The value of diamagnetic term and the paramagnetic coefficient both decrease with increasing the layers of LAO. The larger paramagnetic contribution induces the higher Kondo temperature as seen in Fig. 2(a) and description in the paragraph above.

The resistances below CAR point of 80 K obviously separate during warming up for 15 u.c. LAO/STO sample with applied magnetic field of 0 T and 9 T as seen in Fig. 4(a). Below 80 K, the trapped single oxygen vacancies and oxygen divacancies along the polarized domain walls are localized and carriers are dominated by a few of electrons. Under applied magnetic field the cyclotron precession lengthens the electron path and lifts the resistance. Above 80 K, the trapped vacancies are gradually released, dominate the carriers and recombine with the conducting electrons at low temperature. Because the larger effective mass and smaller mobile velocities of vacancies only induce the tiny cyclotron precessional path, the difference of resistance between non-applied field and applied field can be ignored

above 80 K, as seen in Fig. 4(a). Fig. 4(b) presents the magnetoresistance at different temperature during warming for 15 u.c. LAO/STO sample. The result is clear that the magnetoresistance shows ordinary positive value, and decreases with temperature increasing from 20 K. It is worth mention that the magnetoresistance at 2 K shows clearly two segment distribution, which is known as the weak anti-localization phenomenon.<sup>11,14</sup> At the condition of low temperature and low field, there exists the relation of  $\tau_{\phi} > \tau_B > \tau_{SO}$  (the terms are the relaxation time of electron-phonon scattering, magnetic field and spin-orbital scattering, respectively), therefore the main contribution is spin-orbital scattering. When the field increases and leads to  $\tau_B \approx \tau_{SO}$ , or the temperature increase and makes  $\tau_{\phi} \approx \tau_{SO}$ , the spin-orbital contribution for resistance could disappear, and electron-phonon scattering take places. This also contributes to the saturation of logarithmic term of transport result as mention above.

## Conclusion

The temperature dependent transport and magnetization of LAO/STO with 7, 15 and 25 u.c. layers of LAO were investigated during cooling and warming. The conductivity accelerated



recoveries were observed at 80 K and 176 K for the large electrode area of several mm, which are induced by the oxygen single vacancy and divacancy trapped by the polarized domain walls become mobile at these temperatures. The recoveries are found to be more obvious for more layers LAO sample, which is attributed that the domain walls diffuse along longitudinal direction and expand larger network with increasing vertical strain gradient. The strain modified domain provides a novel method tuning the CAR effect and related transport properties. Due to the stable and precise temperature interval and large scale device, the CAR may provide a potential widely applied temperature standard reference. Paramagnetic and diamagnetic are found to coexistence for the whole temperature range in the as-prepared samples, which is different from the previous reports. The distinction shows the importance of the preparation technique. Also Kondo effect and weak anti-localization were found at low temperature for 7 u.c. and 15 u.c. samples due to the weightier paramagnetic content. Our work helps better understanding the role of strain and domain playing in the LAO/STO heterostructure. The modification of CAR effect and related transport and magnetic properties *via* the control of strain provide important reference value to design the further application devices of LAO/STO.

## Conflicts of interest

There are no conflicts to declare.

## Acknowledgements

This work was supported by the Science Challenge Project (No. TZ2016001), and the National Natural Science Foundation of China (Grant No. 51677175 and 11304300). We thank Dr Long Cheng for providing the high quality samples.

## References

- 1 A. Ohtomo and H. Y. Hwang, *Nature*, 2004, **427**, 423–426.
- 2 N. Reyren, S. Thiel, A. D. Caviglia, L. F. Kourjoutis, G. Hammerl, C. Richter, C. W. Schneider, T. Koop, A.-S. Ruetschi, D. Jaccard, M. Gabay, D. A. Muller, J.-M. Triscone and J. Mannhart, *Science*, 2007, **317**, 1196.
- 3 D. A. Dikin, M. Mehta, C. W. Bark, C. M. Folkman, C. B. Eom and V. Chandrasekhar, *Phys. Rev. Lett.*, 2011, **107**, 056802.
- 4 L. Li, C. Richter, J. Mannhart and R. C. Ashoori, *Nat. Phys.*, 2011, **7**, 762–766.
- 5 J. A. Bert, B. Kalisky, C. Bell, M. Kim, Y. Hikita, H. Y. Hwang and K. A. Moler, *Nat. Phys.*, 2011, **7**, 767–771.
- 6 S. Banerjee, O. Erten and M. Randeria, *Nat. Phys.*, 2013, **9**, 626–630.
- 7 Ariando, X. Wang, G. Baskaran, Z. Q. Liu, J. Huijben, J. B. Yi, A. Annadi, A. Roy Baran, A. Rusydi, S. Dhar, Y. P. Feng, J. Ding, H. Hilgenkamp and T. Venkatesan, *Nat. Commun.*, 2011, **2**, 188–194.
- 8 A. Brinkman, M. Huijben, M. Van Zalk, J. Huijben, U. Zeitler, J. C. Maan, W. G. Van Der Wiel, G. Rijnders, D. H. A. Blank and H. Hilgenkamp, *Nat. Mater.*, 2007, **6**, 493–496.
- 9 F. J. Wong, R. V. Chopdekar and Y. Suzuki, *Phys. Rev. B: Condens. Matter Mater. Phys.*, 2010, **82**, 165413.
- 10 T. Hernandez, C. W. Bark, D. A. Felker, C. B. Eom and M. S. Rzchowski, *Phys. Rev. B: Condens. Matter Mater. Phys.*, 2012, **85**, 161407.
- 11 A. D. Caviglia, M. Gabay, S. Gariglio, N. Reyren, C. Cancellieri and J.-M. Triscone, *Phys. Rev. Lett.*, 2010, **104**, 126803.
- 12 H. L. Guo, W. A. Saidi, J. L. Yang and J. Zhao, *Nanoscale*, 2016, **8**, 6057–6063.
- 13 F. Gunkel, S. Wicklein, S. Hoffmann-Eifert, P. Meuffels, P. Brinks, M. Huijben, G. Rignders, R. Waser and R. Dittmann, *Nanoscale*, 2015, **7**, 1013–1022.
- 14 Z. Zhong, A. Toth and K. Held, *Phys. Rev. B: Condens. Matter Mater. Phys.*, 2013, **87**, 161102.
- 15 D. G. Schlom and J. Mannhart, *Nat. Mater.*, 2011, **10**, 168.
- 16 H. Y. Hwang, *Science*, 2006, **313**, 1895.
- 17 S. Thiel, G. Hammerl, A. Schmehl, C. W. Schneider and J. Mannhart, *Science*, 2006, **313**, 1942.
- 18 G. Herranz, M. Basletic, M. Bibes, C. Carretero, E. Tafra, E. Jacquet, K. Bouzehouane, C. Deranlot, A. Hamzic, J.-M. Broto, A. Barthelemy and A. Fert, *Phys. Rev. Lett.*, 2007, **98**, 216803.
- 19 A. Kalabukhov, R. Gunnarsson, J. Borjesson, E. Olsson, T. Claeson and D. Winkler, *Phys. Rev. B: Condens. Matter Mater. Phys.*, 2007, **75**, 121404.
- 20 S. Nazir, M. Behtash and K. Yang, *Appl. Phys. Lett.*, 2014, **105**, 141602.
- 21 R. Yamamoto, C. Bell, Y. Hikita, H. Y. Hwang, H. Nakamura, T. Kimura and Y. Wakabayashi, *Phys. Rev. Lett.*, 2011, **107**, 036104.
- 22 Y. Chen, N. Pryds, J. E. Kleibeuker, G. Koster, J. Sun, E. Stamate, B. Shen, G. Rijnders and S. Linderorth, *Nano Lett.*, 2011, **11**, 3774–3778.
- 23 C. W. Schneider, M. Esposito, I. Marozau, K. Conder, M. Doebeli, Y. Hu, M. Mallepell, A. Wokaun and T. Lippert, *Appl. Phys. Lett.*, 2010, **97**, 192107.
- 24 S. Nazir, C. Bernal and K. Yang, *ACS Appl. Mater. Interfaces*, 2015, **7**, 5305–5311.
- 25 M. Hosoda, C. Bell, Y. Hikita and H. Y. Hwang, *Appl. Phys. Lett.*, 2013, **102**, 091601.
- 26 H. Yan, Z. Zhang, S. Wang, X. Wei, C. Chen and K. Jin, *ACS Appl. Mater. Interfaces*, 2018, **10**, 14209–14213.
- 27 G. Shirane and Y. Yamada, *Phys. Rev.*, 1969, **177**, 858.
- 28 D. Roy, Y. Frenkwl, S. Davidovitch, E. Persky, N. Haham, M. Gabay, B. Kalisky and L. Klein, *Phys. Rev. B*, 2017, **95**, 245303.
- 29 B. Kalisky, E. M. Spanton, H. Noad, J. R. Kirtley, K. C. Nowack, C. Bell, H. K. Sato, M. Hosoda, Y. Xie, Y. Hikita, C. Woltmann, G. Pfanzelt, R. Jany, C. Richter, H. Y. Hwang, J. Mannhart and K. A. Moler, *Nat. Mater.*, 2013, **12**, 1091.
- 30 Z. Erlich, Y. Frenkel, J. Drori, Y. Shperber, C. Bell, H. K. Sato, M. Hosoda, Y. Xie, Y. Hikita, H. Y. Hwang and B. Kalisky, *J. Supercond. Novel Magn.*, 2015, **28**, 1017–1020.
- 31 H. J. H. Ma, S. Scharinger, S. W. Zeng, D. Kohlberger, M. Lange, A. Stöhr, X. R. Wang, T. Venkatesan, R. Kleiner,



- J. F. Scott, J. M. D. Coey, D. Koelle and Ariando, *Phys. Rev. Lett.*, 2016, **116**, 257601.
- 32 S. Seri, M. Schultz and L. Klein, *Phys. Rev. B: Condens. Matter Mater. Phys.*, 2012, **86**, 085118.
- 33 S. Seri, M. Schultz and L. Klein, *Phys. Rev. B: Condens. Matter Mater. Phys.*, 2013, **87**, 125110.
- 34 M. Z. Minhas, A. Muller, F. Heyroth, H. H. Blaschek and G. Schmidt, *Sci. Rep.*, 2017, **7**, 5215.

